Brain Stimulation 11 (2018) 1044–1053

Contents lists available at ScienceDirect

Brain Stimulation

journal homepage: http://www.journals.elsevier.com/brain-stimulation

Dry tDCS: Tolerability of a novel multilayer hydrogel composite non-adhesive electrode for transcranial direct current stimulation

Niranjan Khadka [a], Helen Borges [a], Adantchede L. Zannou [a], Jongmin Jang [b], Byunggik Kim [b], Kiwon Lee [b], Marom Bikson [a, *]

[a] Department of Biomedical Engineering, The City College of New York, CUNY, New York, NY, 10031, USA
[b] Ybrain Inc, Seongnam-si, Republic of Korea

A R T I C L E I N F O

Article history:
Received 30 May 2018
Received in revised form
17 July 2018
Accepted 18 July 2018
Available online 29 July 2018

Keywords:
Dry electrode
tDCS
Tolerability
Erythema

A B S T R A C T

Background: The adoption of transcranial Direct Current Stimulation (tDCS) is encouraged by portability and ease-of-use. However, the preparation of tDCS electrodes remains the most cumbersome and error-prone step. Here, we validate the performance of the first "dry" electrodes for tDCS. A "dry electrode" excludes 1) any saline or other electrolytes, that are prone to spread and leaving a residue; 2) any adhesive at the skin interface; or 3) any electrode preparation steps except the connection to the stimulator. The Multilayer Hydrogel Composite (MHC) dry-electrode design satisfied these criteria.

Objective/Hypothesis: Over an exposed scalp (supraorbital (SO) regions of forehead), we validated the performance of the first "dry" electrode for tDCS against the state-of-the-art conventional wet sponge-electrode to test the hypothesis that whether tDCS can be applied with a dry electrode with comparable tolerability as conventional "wet" techniques?

Methods: MHC dry-electrode performance was verified using a skin-phantom, including mapping voltage at the phantom surface and mapping current inside the electrode using a novel biocompatible flexible printed circuit board current sensor matrix (fPCB-CSM). MHC dry-electrode performance was validated in a human trial including tolerability (VAS and adverse events), skin redness (erythema), and electrode current mapping with the fPCB-CSM. Experimental data from skin-phantom stimulation were compared against a finite element method (FEM) model.

Results: Under the tested conditions (1.5 mA and 2 mA tDCS for 20 min using MHC-dry and sponge-electrode), the tolerability was improved, and the erythema and adverse-events were comparable between the MHC dry-electrode and the state-of-the-art sponge electrodes.

Conclusion: Dry (residue-free, non-spreading, non-adhesive, and no-preparation-needed) electrodes can be tolerated under the tested tDCS conditions, and possibly more broadly used in non-invasive electrical stimulation.

1. Introduction

Transcranial direct current stimulation (tDCS) is a non-invasive brain stimulation tool used in healthy and patient populations where a weak direct current (1–2 mA) is applied through two or more electrodes placed on the scalp [1], [2]. A major contributor to the rapid and broad adoption of tDCS is portability and ease-of-use. tDCS is well tolerated with common mild side-effects such as transient cutaneous sensations (for e.g. as warmth, itching, and tingling) and erythema [3–7]. However, when (and only when) established standard protocols are not followed [8], tDCS can produce significant skin irritation [9–12]. Given that cutaneous sensation and irritation are the primary risks of tDCS [3] [7] [13], [14], proper electrode preparation and monitoring are vital for tolerability and reproducibility [4] [6], [15]. Yet, the preparation and placement of tDCS electrodes remain the most cumbersome and prone-to-error steps [7]. For example, both the level of sponge fluid saturation and head-gear tightness need to be titrated to balance good skin contact while avoiding of saline spread, and sponges can dehydrate or move [16] over an extended time. Thus, despite success with current research/clinical grade equipment and

* Corresponding author. Department of Biomedical Engineering, The City College of New York, CUNY, 160 Convent Avenue, New York, NY, 10031, USA.
E-mail address: bikson@ccny.cuny.edu (M. Bikson).

https://doi.org/10.1016/j.brs.2018.07.049
1935-861X/

accessories, even for remote-supervised home use [17], there is an interest to continue to enhance technology to deploy tDCS.

The sponge-pocket style electrode (25–35 cm^2) with conductive rubber insert, pin connectors, and saline application by the operator is the most traditional tDCS electrode used [16] [18], but most prone to preparation error, notably when poor materials are used by insufficiently trained users [19]. Circular sponges do not appear to provide an advantage [14], [20]. The introduction of pre-saline-saturated snap-connector sponge electrodes [21] automates most of the sponge electrode preparation process. Electrolyte gel or paste is used in specialized tDCS application (e.g. in MRI [22]). Specialized adhesive hydrogels electrodes can support tDCS [4]. High-Definition electrodes with a distinct small form factor (~1 cm diameter [23]) use specialized hydrogels [24]. What all these electrodes design share, is a "wet" electrode-skin-interface, where a fluid or viscous electrolyte is assumed to saturate the skin [25], which in turn result in some residue on the skin.

Here, we validate the performance of the first "dry" electrodes for tDCS. Dry electrodes exclude: 1) any saline or other conductive hydrogel-based gel or paste, that are prone to leak or spread, and that leave a residue; 2) any adhesive at the skin, either around the electrode or part of the hydrogel; or 3) any electrode preparation steps by the operator except connection to the stimulator. A novel Multilayer Hydrogel Composite (MHC) electrode design fulfills these criteria. FEM models and a skin-phantom were used to verify electrode performance followed by tolerability validation in healthy subjects. Adverse events, erythema, and VAS pain were scored using established protocols [4] [7] [10], [13], [26]. In addition, we developed a biocompatible flexible printed circuit board current sensor matrix (fPCB-CSM) to map current distribution inside the electrode during phantom or subject stimulation. In all experiments, MHC dry-electrode performance was compared against a state-of-the-art sponge electrode to address the hypothesis: can tDCS be applied with a dry electrode with comparable tolerability as conventional "wet" techniques.

2. Materials and methods

This study involves experimental measures in phantom (voltage) and participants (via VAS and adverse events reporting questionnaire), computational FEM simulation in phantom, current mapping in the electrode, and an algorithm based image processing of erythema distribution.

2.1. Participants

The study was conducted in accordance with the protocols and procedures approved by the Institutional Review Board of the City College of New York, CUNY. Twenty healthy participants (13 males and 7 females; age 19–34 years; mean age 24.7 ± 4.9) completed this study. Volunteers with any sign of skin disorder/sensitive skin (ex. eczema, severe rashes), blisters, open wounds, burn including sunburns, cuts or irritation (e.g. due to shaving), or other skin defects which compromise the integrity of the skin at or near stimulation locations were excluded from this study. However, participants on mild acne medication with non-irritating skin disorders were not excluded. Similarly, prospective volunteers with any neuropsychiatric disorders or receiving medication for such disorders were excluded from this study. Participants volunteered in four different tDCS sessions using 1.5 mA and 2 mA current intensities plus an additional two sessions at 2 mA with the fPCB-CSM for both MHC dry and sponge-electrodes in a randomized order. All participants provided written informed consent to participate in the study. Participants were seated in an upright relaxed position and performed a lexical decision task throughout the duration of the stimulation.

2.2. Novel sensor array

The current sensor made up of a novel biocompatible flexible printed circuit board current sensor matrix (fPCB-CSM) comprises

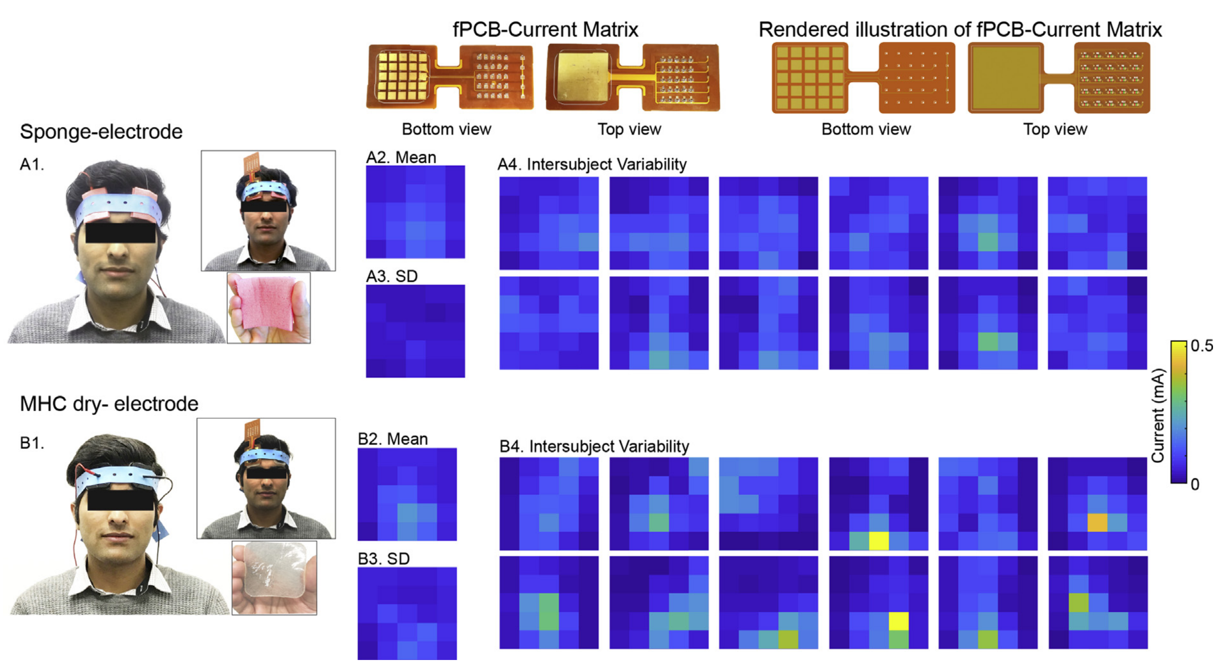

Fig. 1. A configuration of conventional sponge and MHC-dry electrode, with and without fPCB within-electrode current mapping sensor. and voltage map represented as false colormap measured in the electrode using fPCB voltage sensor. (A1, B1) Electrical stimulation set-up on a participant's forehead using a bifrontal (left/right SO) montage electrode configuration. A biocompatible rubber strap secured both electrode types on the forehead and the electrodes were connected to the stimulator. In some experiments, a customize novel fPCB current mapping sensor array unit (bottom panel of B1) positioned inside the electrode mapped at the different location of electrode plane during tDCS. Current mapping data measured from 12 participants for either electrode type (false colormap for each sensor).

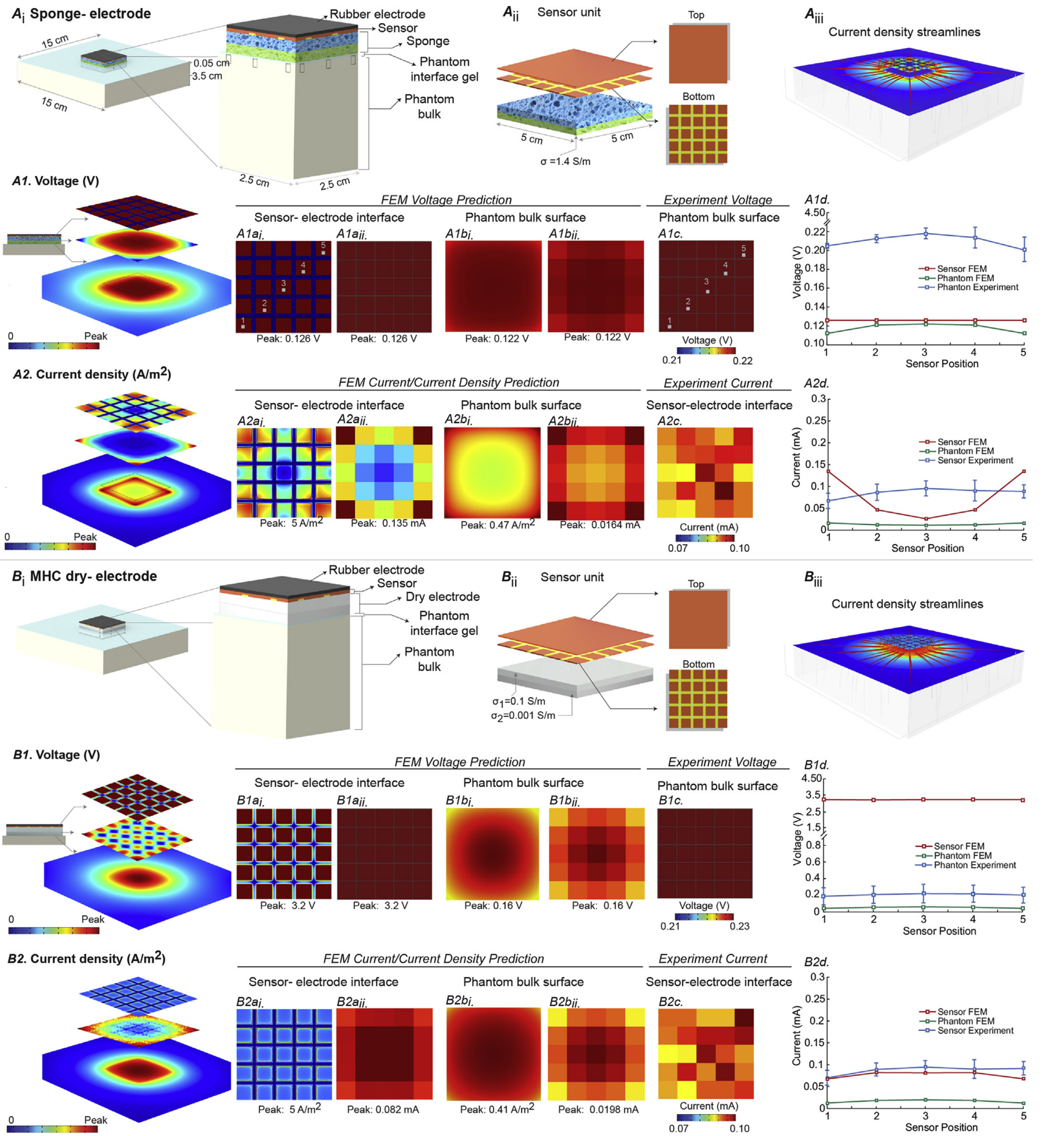

Fig. 2. Electrical performance of conventional sponge-electrode and MHC dry electrode verified using a skin-phantom and FEM simulations. Phantom voltages and electrode currents were measured using the Ag/AgCl array or fPCB-CSM, respectively, with corresponding FEM prediction. (A_i) Architecture of a phantom model showing expanded cut off view of rubber electrode, sensor array, and sponge-electrode assembly on the phantom-gel surface. (A_{ii}) illustration of fPCM-CSM sensor unit positioned over sponge pad. (A_{iii}) represents an orientation of current density flow streamlines from inside of the electrode to the phantom. (*A1*) Voltage distribution measured experimentally and predicted by FEM simulation at the sensor-electrode interface and phantom bulk surface. The leftmost panel of *A1* illustrates side-view of the electrode-sensor and phantom assembly, and predicted voltage distribution at the sensor-electrode interface (dorsal), within-sponges (medial), and phantom bulk surface (ventral). Middle row of *A1* shows FEM prediction of voltage distribution at the sensor-electrode interface and phantom bulk surface using simulation result ($A1a_i$, $A1b_i$) and false voltage distribution map at each small squared surface that resemble the shape of the experimental sensor arrays ($A1a_{ii}$, $A1b_{ii}$) and the measured voltage from experimental measures (*A1c*). Peak FEM predicted voltage at the sensor-electrode interface was 0.126 V and 0.122 V at the phantom bulk surface. Experimental voltage measurement at the phantom bulk surface was 0.22 V (peak). (*A1d*) Graphical representation of voltage line graphs plotted from diagonal voltage components at the sensor-electrode interface and phantom bulk surface (FEM prediction results), and an experimental measure. Position of the sensors is represented as numbers in a diagonal fashion as illustrated in $A1a_i$, $A1b_i$ and *A1c*. Results represents an overall distribution map of voltage. (*A2*) represents current/current density measured experimentally and predicted by the FEM simulation at the sensor-electrode interface and phantom bulk surface. Panel at the left of *A2* shows stacked view of current density distribution from sensor-electrode interface (dorsal), within-sponges (medial), and phantom bulk surface (ventral). FEM prediction of current/current density and experimental measurement of current are shown in the middle panel of *A2*. Peak current of 5 A/m^2 (*A2a*) and a peak current of 0.135 mA ($A2a_{ii}$) was predicted at the sensor-electrode interface, whereas at the phantom bulk surface FEM predicted a peak current density of 0.47 A/m^2 ($A2b_i$) and a peak current of 0.0164 mA ($A2b_{ii}$). Current measured experimentally (*A2c*) at the sensor-electrode interface was almost uniform. (*A2d*) Representation of line plots of diagonal current measured experimentally and predicted by FEM at sensor-electrode interface and phantom bulk surface. (B_i) Illustration of MHC dry electrode positioning over the phantom-gel surface. (B_{ii}) schematics of the sensor array

two units: 1) measuring unit (top view) and 2) sensor unit (bottom view) (Fig. 1, Fig. 2A and B). The measuring unit (rubber electrode positioning side) of the novel sensor array has an exposed gold (Au) plated uniform copper (Cu) metal surface, whereas on its distal side, there are twenty-five 50 Ω soldered resistors (5 rows and 5 columns of resistors) and five common grounds for each row. The sensor unit underneath the measuring unit (sponge/MHC-dry electrode side) has a high heat resistance polyimide insulating substrate that divides the conductive metal into twenty-five small sensor electrode arrays. Each of these twenty-five sensor arrays is connected independently to the twenty-five test resistors located at the measuring unit. Each end of the sensor array has a dimension of 5 cm × 5 cm x 0.03 cm (Fig. 1). The entire sensor array is assembled into one compound unit using a biocompatible polyimide substrate.

2.3. Voltage sensor array for phantom study

Twenty-Five Ag/Agcl pellet shaped electrodes (diameter = 1 mm) were embedded inside an agar phantom (based on [27] [28]) such that the planar assembly mimics the shape of an overlaid 5 × 5 cm^2 tDCS electrode, and the position of each electrode corresponds to the center of the 25-small fPCB-CSM sensor arrays. An embedded reference electrode placed 5 cm away from the twenty-five electrode array was used as a ground for voltage measurement across the recording electrodes.

2.4. MHC dry-electrode

The dual layer structure of the MHC dry-electrode includes independently optimized mechanical, electrical, and chemical properties of the hydrogel. The top layer (thickness, 0.6 mm) of the MHC dry-electrode was composed of an adhesive polymer hydrogel, whereas the bottom layer (thickness, 1 mm) had a non-adhesive bio-compatible polymer hydrogel containing Poly-Vinyl Alcohol (PVA) (Fig. 1). Both layers were optimized in a way that the top layer becomes less resistive to redistribute the injected current across the electrode plane, whereas the bottom layer becomes highly resistive layer and minimizes current clustering at the skin [18]. Furthermore, any electrochemical produced (e.g. pH changes) at the electrode (non-ionic/ionic conduction) interface within the electrodes were optimized using the top layer as a diffusion barrier [25]. The electrode components weight by percentage) were: *cross-linked acrylic resin* (top layer: 15–25; bottom layer: 15–25); *polyhydric alcohol* (top layer: 40–60; bottom layer: 30–60); NaCl as an *electrolytic salt* (top layer: < 10; bottom layer: < 8); *additives/stabilizers* (top layer: < 0.5; bottom layer: < 0.5); *deionized water* (top layer: 20–40; bottom layer: 20–40); *polyvinyl alcohol res*in (top layer: none; bottom layer: 1–5).

The effectiveness of the MHC dry-electrode was successfully evaluated not only as a current re-distribution layer but also as a diffusion barrier layer [29]. In the diffusion barrier test, pH changes were measured at the entire conductive silicone rubber/top hydrogel layer, top/bottom hydrogel layer, and bottom hydrogel layer/skin interface after 2 mA 30min stimulation. There was no pH change at the bottom/skin hydrogel interface. Only less than 0.3% of the total electrode area showed pH change at the top/bottom hydrogel layer interface (n = 30).

2.5. Electrode preparation and placement

The experiment was conducted on rectangular phantom bulks (15 cm × 8 cm x 5 cm; prepared using established standard protocols as discussed in Ref. [27] [28]). Prior to the electrode placement, a thin coat (~0.5 cm) of conductive electrode gel (Signa gel, Parker Laboratories Inc., NJ, USA) was applied over the agar phantom bulk. Conductive gel was used to maintain a consistent contact between the stimulation electrodes and the phantom. For the phantom study, the conventional sponge-electrode (5 × 5 cm) were first soaked with saline (0.9% NaCl) and a conductive carbon rubber (5 × 5 cm, Carbon Rubber Electrode, Soterix medical Inc., NY, USA) was inserted inside the sponge pocket. While the whole assembly is often referred as an electrode in tDCS, the electrode is technically the conductive rubber and the saline/gel is technically the electrolyte [19]. Two electrodes (anode and cathode; 5 × 5 cm each) were then positioned on the phantom with an interelectrode distance of 10 cm and connected to a tDCS stimulator (1 × 1 tDCS, Soterix Medical Inc., NY, USA). The non-adhesive bottom layer of the MHC dry-electrode was placed over the phantom bulk and a conductive silicone rubber was positioned on the top adhesive layer of the MHC-dry electrode which was connected to the tDCS device.

For the human study, a bifrontal montage (anode left and cathode right on the supraorbital (SO) region of a forehead) was used to place both type of electrodes. Note that we selected this particular montage to overcome the major limitation of the MHC dry-electrode- not applicable in hairy regions of scalp unlike the conventional "wet" sponge-electrode. Electrodes were positioned and secured over the brain region using an elastic fastener (Soterix Medical Elastic Fastener, Soterix Medical Inc., NY, USA).

When current at the electrode was measured, the fPCB-CSM array was placed in between the sponge or MHC dry-electrode (bottom) and the conductive carbon/silicone rubber electrode (top). Together they formed a stacked electrode configuration of rubber electrode, fPCS-CSM array, and sponge/MHC dry-electrode respectively.

2.6. Stimulation and current/voltage measurement

A weak 1.5 or 2 mA direct current (with an additional linear ramp up and down of 30 s at the beginning and at the end of stimulation) from a tDCS stimulator was applied in both human and phantom studies through sponge or MHC dry-electrodes. In the human study, voltage was measured across each test resistor located at the measuring unit of the fPCB-CSM using a digital multimeter (Fluke 87 V Industrial Multimeter, Fluke Corporation, WA, USA) and the corresponding current was calculated using the Ohm's law. In the phantom bulk experiment, voltage was measured across the twenty-five embedded recording electrodes using a low power instrumentation amplifier (AD620, Analogue Devices, MA,

rendered on top of the MHC dual-layered (top layer: *0.1 S/m* and bottom layer: *0.001 S/m*) dry electrode. (B_{iii}) represents uniformly seeded current density streamlines distribution from the surface of rubber electrode to the phantom. Left panel of *B1* shows slice view of electrode assembly and FEM predicted voltage at the sensor-electrode interface, within-MHC dry electrode, and phantom bulk surface. Middle panel of *B1* is an illustration of voltage distribution as predicted by FEM simulation (Sensor-electrode interface: $B1a_i$, $B1a_{ii}$ and phantom bulk surface: $B1b_i$, $B1b_{ii}$) and measured experimentally (*B1c*). Peak predicted voltage was 3.2 V at the sensor-electrode interface and 0.16 V at the phantom bulk surface, whereas experimentally, a comparable peak voltage of 0.23 V was measured as that of the sponge-electrode. Line plots of voltages shows even voltage distribution in the diagonal direction. (*B2*) Stacked slices of current density distribution at the sensor-electrode interface, within the MHC electrode, and at the phantom bulk surface (left panel). A comparable peak current density of 5 A/m^2 as that in the sponge electrode was predicted at the sensor-electrode interface ($B2a_i$) whereas mean peak current was 0.082 mA (B2a*ii*). Predicted current density ($B2b_i$) and current ($B2b_{ii}$) at the phantom bulk surface was comparable to that of the sponge-electrode and the distribution was almost uniform (slightly higher at the center but without edges). Comparable current as in the conventional sponge electrode was measured at the senor-electrode interface (*B2c*). Diagonal current distribution line graph was almost identical to that of conventional sponge electrode (*B2d*).

USA), whereas current at the electrode was measured using the aforementioned procedure as in the human study. Note that for current measurement at the electrode in both human study and phantom study, the fPCB-CMS was positioned over the sponge or MHC dry-electrode and the carbon/silicone rubber electrode was placed on the top surface of the sensor.

2.7. Pain and adverse events

Headache, neck pain, scalp pain, tingling, burning sensation, itching sensation, sleepiness, trouble concentrating, dizziness, and nausea were assessed through self-reporting questionnaires completed by the participants before and after each session (Table 1). The intensity of the events was rated from 1 - 4 (1 = absent, 2 = mild, 3 = moderate, and 4 = severe) and their relationship to tDCS was rated in a scale from 1 - 5 (1 = none, 2 = remote, 3 = possible, 4 = probable, and 5 = definite). A visual analogue scale (VAS) was used during the 20 min 1.5 mA or 2 mA stimulations to report skin sensation or pain (if any) in a scale of 1–10 (1: no or minimum pain and 10: unbearable pain). Stimulation was aborted if a participant reported a VAS of 7 or above. The VAS for pain was collected during the stimulation, while the participants were performing the lexical decision task. The lexical decision task was presented as a mixture of words (e.g. house, ship, sleep, etc.) and pseudowords (nonsense strings that represented the phonotactic rules of a language, like trud in English) and participants reported whether the presented stimulus was a word or a pseudoword. The lexical decision task was paused every 2 min to allow participants time to report the VAS.

2.8. Computational model and solution method

The phantom was modeled as a homogenous and isotropic volume conductor of dimension 15 cm × 15 cm x 3.55 cm (including a 0.5 mm thin layer of conductive gel). Computer-aided design models of phantom bulk, conductive gel, sponge or MHC dry-electrode, sensor arrays, and rubber electrode (Figs. 2 and 3) were modeled in SolidWorks (2013) (Dassault Systemes Americas Corp., MA, USA) and were assembled in ScanIP software (Synopsys, Exeter, UK). Dimensions of rubber electrode, MHC dry-electrode, sponge, and sensor arrays were based on the experimental values. An adaptive tetrahedral meshing algorithm was implemented in ScanIP to generate meshes of the phantom bulk for both conventional sponge-electrode and MHC dry-electrode simulation cases. The finite element method (FEM) models of the volumetric meshes were then imported and solved in COMSOL Multiphysics 4.3 (COMSOL, Inc., MA, USA) using electric current physics at a steady-state assumption. The final FEM phantom model was solved for greater than 600,000° of freedom and had greater than 400,000 tetrahedral elements. The phantom conductivities were based on prior literature [28]. The Laplace equation ($\nabla (\sigma \nabla V) = 0$ where 'V' is potential, 'σ' is conductivity) was solved to simulate direct current stimulation. Boundary conditions for phantom simulation were applied as uniform normal current density (inward current flow: J_{norm}) at the top exposed surface of the anode (2 mA) and ground at the bottom surface of the phantom bulk layer. All other external surfaces of the phantom bulk model were electrically insulated. Two versions of MHC dry-electrodes with varying electrical conductivities of the top and bottom layers were simulated (MHC dry-electrode Variation I and II; Fig. 3).

2.9. Image post processing and analysis

The photographs of participant's forehead (area under anode) taken immediately after stimulation were analyzed for erythema distribution using a customized MATLAB (MathWorks, MA, USA) based image processing graphical user interface (GUI) as previously illustrated in Ref. [26] (Fig. 4).

2.10. Statistical tests

Normality of the VAS, cumulative adverse events responses, and adverse events in relationship to tDCS were tested using Shapiro-Wilk tests with Lilliefors significance correction across electrode types (dry-electrode vs. sponge-electrode) and stimulation intensities (1.5 mA vs. 2 mA). A corresponding non-parametric test (Wilcoxon signed rank test) or a parametric test (repeated measures ANOVA) probed significance of the data. A critical value (α) of 0.05 was accepted as a significant difference between groups.

3. Results

Voltage and current density/current distribution at the sensor-electrode interface and phantom bulk surface during direct current stimulation (2 mA, 20 min) were predicted by FEM simulation (phantom) and measured experimentally (phantom gel and *in vivo* study) using both conventional sponge-electrode and MHC dry-electrode. In addition, VAS score, lexical decision task response, and adverse event analysis based on participants' rating and response were analyzed.

3.1. In vivo current mapping

The fPCB-CSM mapped the overall current distribution inside both sponge-electrode and MHC dry-electrode with 2 mA tDCS. The distribution was represented as a heat map (mean and standard deviation, or intersubject variability) where each square represents current at one sensor position (Fig. 1A2, 1A3, 1A4: Sponge-electrode and 1B2, 1B3, 1B4: MHC dry-electrode). The total current across all fPCM-CSM sensors was 2 mA in all cases, as expected. Across individuals, there was no evident concentration of current at any fPCM-CSM sensor or sensors, for either MHC dry-electrode or sponge-electrode. On an individual basis, hot spots (e.g. 6× average) were detected but with no consistent pattern suggesting that it reflect idiosyncratic contact of the electrode with the skin surface or internal skin or electrode inhomogeneities. In any case, there was no average or individual electrode observation of current concentration at the electrode edge (at sensors around the perimeter) as much be predicted based on prior models [14] [18], [30–32].

3.2. Erythema distribution

Erythema was diffused across the skin-electrode contact area in both MHC dry-electrode and sponge-electrode for both stimulation intensities as indicated by the probability heat map. For the MHC dry-electrode, the peak cumulative probability of erythema distribution for 1.5 mA was 50%; 41.2% for mild and 17.65% for strong (Fig. 4B1) whereas for 2 mA (Fig. 4B2), the cumulative erythema percentage was 73.53%; 52.9% for mild and 32.35% for strong. Conventional sponge-electrode had the peak probability of 50% erythema distribution for 1.5 mA (Fig. 4B3); 50% for mild and 18.9% for strong, and for 2 mA (Fig. 4B4), the peak cumulative erythema was 71.1%; 57.9% for mild and 26.32% for strong. The mean probability of erythema distribution yielded by MHC dry-electrode and conventional sponge-electrode were comparable (Fig. 4).

Performance of conventional sponge-electrode and MHC dry-electrode with variations: FEM prediction and Experimental Measures.

Table 1
Representation of adverse events as intensity and relationship to tDCS based on subjective reporting before and after stimulation (pre- and post). Reporting of adverse events (mean ± SD) were comparable across electrode types and stimulation intensities.

		Adverse Events	Headache	Neck pain	Scalp pain	Tingling	Burning Sensation	Itching	Sleepiness	Trouble concentrating	Dizziness	Nausea
Sponge-electrode	1.5 mA	Reports	3	2	0	11	7	9	8	7	1	1
		(%)	(15%)	(10%)		(55%)	(35%)	(45%)	(40%)	(35%)	(5%)	(5%)
		Intensity (mean ± SD)	(1.20 ± 0.52)	(1.10 ± 0.30)	(1.0 ± 0.0)	(1.70 ± 0.73)	(1.50 ± 0.76)	(1.76 ± 0.83)	(1.60 ± 0.99)	(1.50 ± 0.82)	(1.05 ± 0.22)	(1.05 ± 0.24)
		Relation (mean ± SD)	(1.40 ± 0.99)	(1.20 ± 0.61)	(1.0 ± 0.0)	(2.45 ± 1.66)	(2.0 ± 1.52)	(2.35 ± 1.76)	(1.50 ± 1.14)	(1.60 ± 1.09)	(1.15 ± 0.67)	(1.0 ± 0.0)
	2 mA	Reports	2	0	3	9	7	9	5	6	1	0
		(%)	(10%)		(15%)	(45%)	(35%)	(45%)	(25%)	(30%)	(5%)	
		Intensity (mean ± SD)	(1.15 ± 0.48)	(1.0 ± 0.0)	(1.15 ± 0.36)	(1.70 ± 0.92)	(1.50 ± 0.76)	(1.73 ± 0.93)	(1.40 ± 0.82)	(1.35 ± 0.58)	(1.05 ± 0.22)	(1.0 ± 0.0)
		Relation (mean ± SD)	(1.05 ± 0.22)	(1.0 ± 0.0)	(1.40 ± 1.09)	(2.15 ± 1.63)	(1.80 ± 1.32)	(2.05 ± 1.54)	(1.1 ± 0.30)	(1.35 ± 0.74)	(1.05 ± 0.22)	(1.0 ± .00)
MHC dry-electrode	1.5 mA	Reports	3	0	1	9	4	8	5	5	0	1
		(%)	(15%)		(5%)	(45%)	(20%)	(40%)	(25%)	(25%)		(5%)
		Intensity (mean ± SD)	(1.40 ± 0.52)	(1.0 ± 0.0)	(1.05 ± 0.22)	(1.50 ± 0.60)	(1.25 ± 0.55)	(1.64 ± 0.78)	(1.35 ± 0.74)	(1.25 ± 0.44)	(1.0 ± 0.0)	(1.05 ± 0.24)
		Relation (mean ± SD)	(1.05 ± 0.22)	(1.0 ± 0.0)	(1.0 ± 0.44)	(2.20 ± 1.50)	(1.55 ± 1.23)	(2.29 ± 1.64)	(1.05 ± 0.22)	(1.20 ± 0.69)	(1.0 ± 0.0)	(1.0 ± 0.0)
	2 mA	Reports	1	2	0	11	8	9	4	5	0	3
		(%)	(5%)	(10%)		(55%)	(40%)	(45%)	(20%)	(25%)		(15%)
		Intensity (mean ± SD)	(1.05 ± 0.22)	(1.10 ± 0.30)	(1.0 ± 0.0)	(1.65 ± 0.67)	(1.45 ± 0.60)	(1.73 ± 0.93)	(1.30 ± 0.73)	(1.30 ± 0.57)	(1.0 ± 0.0)	(1.15 ± 0.36)
		Relation (mean ± SD)	(1.0 ± 0)	(1.05 ± 0.22)	(1.0 ± 0)	(2.40 ± 1.53)	(2.10 ± 1.51)	(2.42 ± 1.74)	(1.05 ± 0.22)	(1.25 ± 0.71)	(1.0 ± 0.0)	(1.10 ± 0.30)

For Sponge-electrode, the FEM model predicted a peak voltage of 0.126 V at the sensor-electrode interface (Fig. 2*A1a$_i$*, 2*A1a$_{ii}$*) and 0.122 V (peak) at the phantom bulk surface (Fig. 2*A1b$_i$*, 2*A1b$_{ii}$*). An embedded electrode array positioned at the phantom bulk surface measured a maximum voltage of 0.22 V (Fig. 2*A1c*). Predicted voltage and experimentally measured voltage (Mean ± SD) distribution line plots were almost even across diagonal direction (Fig. 2*A1d*), however at the center of the phantom bulk surface, it was slightly higher. The FEM model of sponge-electrode predicted a peak current density of 5 A/m^2 and a peak current of 0.135 mA at the sensor-electrode interface, whereas at the phantom bulk surface, the predicted peak current density and peak current were 0.47 A/m^2 (Fig. 2*A2b$_i$*) and 0.0164 mA (Fig. 2*A2b$_{ii}$*) respectively. Maximum current measured experimentally at the sensor-electrode interface for sponge-electrode was 0.10 mA and the overall current distribution was uniform (Fig. 2*A2c*). However, the FEM model predicted somewhat higher current density/current at the edges (Fig. 2*A2d*).

For MHC dry-electrode, the predicted peak voltage at the sensor-electrode interface was 3.2 V (Fig. 2*B1a$_i$*, Fig. 2*B1a$_{ii}$*) and 0.16 V at the phantom bulk surface (Fig. 2*B1b$_i$*, Fig. 2*B1b$_{ii}$*), higher than the conventional sponge-electrode. The experimental voltage measured at the phantom bulk surface during MHC dry-electrode stimulation was comparable to that of sponge-electrode (Fig. 2*B1c* and Fig. 2*A1c*). The FEM model predicted peak current density and current were 5 A/m^2 and 0.082 mA at the sensor-electrode interface and 0.41 A/m^2 and 0.0198 mA at the phantom bulk surface (Fig. 2*B2a$_i$* and Fig. 2*B2a$_{ii}$*, and Fig. 2*B2b$_i$* and Fig. 2*B2b$_{ii}$*) for the MHC dry-electrode. Overall current distribution at the phantom bulk surface was almost uniform, with peaks around the center (Fig. 2*B2b$_i$*). Current distribution measured experimentally during MHC was comparable to that of conventional sponge-electrode (Max: 0.10 mA, Fig. 2*B2c*).

In MHC dry-electrode Variation I, the FEM predicted similar voltage and current density/current distribution as that of the original MHC dry-electrode (Figs. 2 and 3). However, results from MHC variation II were lower than that of the original configuration of dual hydrogel layers. In MHC variation II, the peak voltages at the sensor electrode interface and phantom bulk surface were 0.19 V and 0.15 V (Fig. 3*B1a$_i$*, Fig. 3*B1a$_{ii}$*, and Fig. 3*B1b$_i$*, Fig. 3*B1b$_{ii}$*), and the predicted peak current density and current at the sensor electrode interface and phantom bulk surface were 5 A/m^2 and 0.0855 mA, and 0.35 A/m^2 and 0.0168 mA respectively (Fig. 3*B2a$_i$*, Fig. 3*B2a$_{ii}$*, and Fig. 3*B2b$_i$*, Fig. 3*B2b$_{ii}$*).

3.3. Tolerability

A total of 120 treatment sessions were conducted, including the *in vivo* current mapping study. No serious adverse events were reported. Eight participants withdrew from the study: six participants withdrew due to scheduling issues (i.e. inability to meet scheduling criterion for a minimum of four sessions), one participant withdrew due to itching during a 2 mA MHC dry session (the only withdrawal during a session), and one participant withdrew without stating a reason. Thus, all but one withdrawal were between-sessions. In total, twenty subjects completed the entire study and group level analysis were conducted on only these 20 subjects. tDCS adverse events were assessed by a self-report questionnaire immediately post-stimulation period (session-wise data, Table 1). The most common adverse events with the highest incidence across all treatment groups were skin tingling, burning, and itching sensations. The cumulative adverse events across stimulation intensities (1.5 mA ($Mdn = 1$) Vs 2 mA ($Mdn = 1$)) when analyzed using the Wilcoxon signed-rank test (non-parametric test) were not significantly different ($Z = -0.003$, $P = 0.997$),

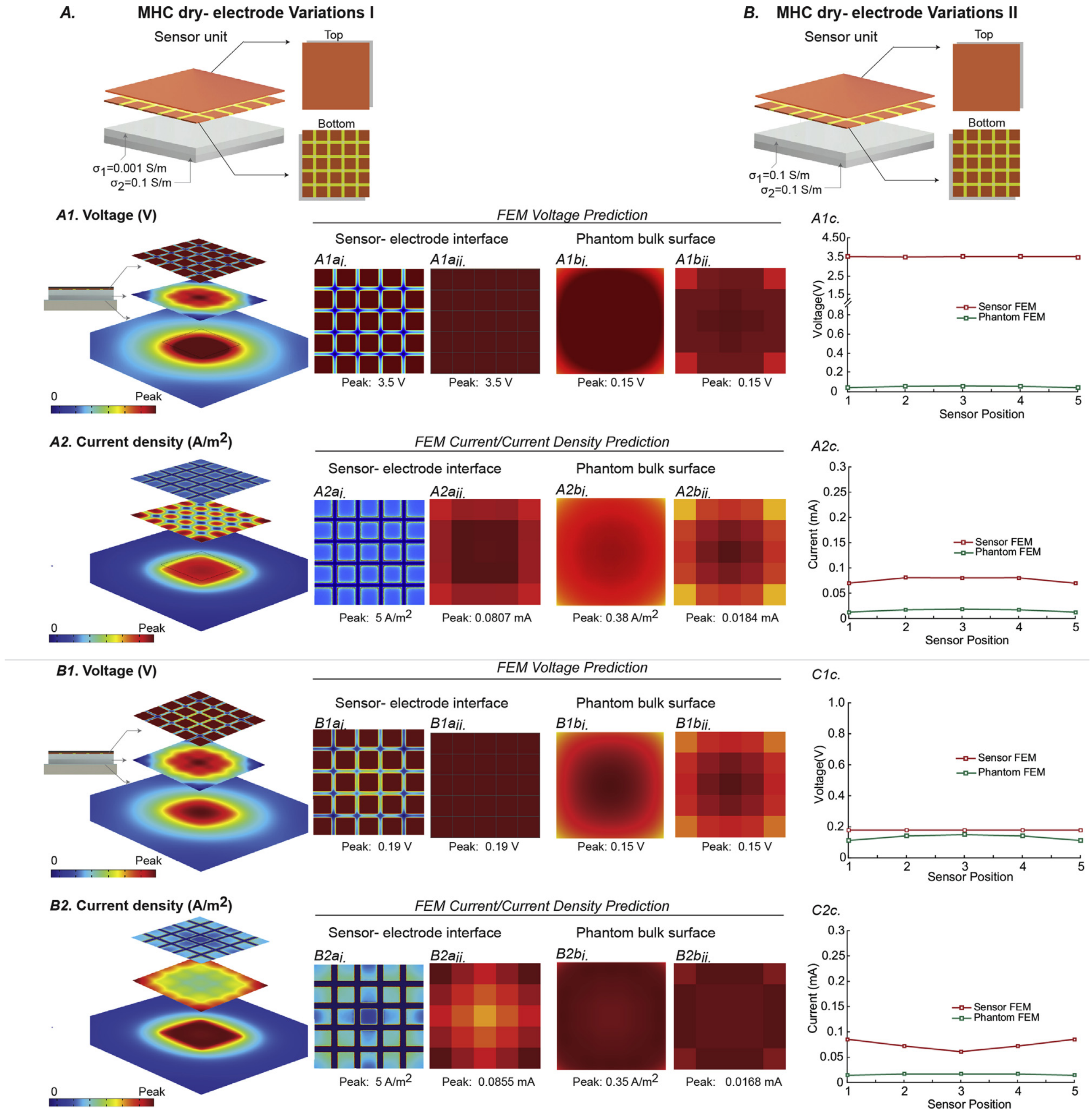

Fig. 3. Performance of MHC dry electrode with variations in electrical conductivities of the dual layers. Voltage and current/current density distribution as predicted by FEM at the sensor-electrode interface and the phantom bulk surface are represented. (*A*) Illustration of voltage distribution at the sensor-electrode interface and phantom bulk surface when the conductivities of the dual layers are reversed (**MHC dry-electrode Variation I**: top layer: *0.001 S/m* and bottom layer: *0.1 S/m*). Stacked slice view of voltage distribution from dorsal to ventral end of the MHC Variation I electrode-phantom assembly (left panel). FEM model predicted a comparable voltage at the sensor-electrode interface ($A1a_i$, $A1a_{ii}$) and phantom bulk surface ($A1b_i$, $A1b_{ii}$) as that of the actual MHC dry electrode. (*A2*) represents current density and current distribution as predicted by FEM simulation. The overall distribution of current density and current was analogous to the MHC dry-electrode ($A2a_i$, $A2a_{ii}$, $A2b_i$, $A2b_{ii}$, *A2c*). (*B*) Voltage and current density/current distribution with **MHC dry-electrode Variation II** (top layer and bottom layer: *0.1 S/m*). The left panel of *B1* represents a distribution of voltage at the sensor-electrode interface and phantom bulk surface. FEM simulation predicted slightly lower peak voltage (0.19 V) at the sensor-electrode interface compared to the actual MHC dry-electrode ($B1a_i$, $B1a_{ii}$), whereas peak voltage at the phantom bulk was comparable ($B1b_i$, $B1b_{ii}$). Representation of current density distribution at different interfaces (*B2*). The simulation predicted comparable current density ($B2a_i$) and current ($B2a_{ii}$) at the sensor-electrode interface, however, at the phantom bulk surface, current density ($B2b_i$) and current ($B2b_{ii}$) was slightly lower than that of MHC dry electrode. (*B2c*) represents variation in current at the sensor-electrode interface and phantom bulk surface.

whereas across electrode types (MHC dry-electrode ($Mdn = 1$) Vs sponge-electrode ($Mdn = 1$)), the adverse events were higher for the sponge-electrode ($Z = -2.344$, $P = 0.019$) (Fig. 5). When analyzed the interaction between the electrode types and stimulation intensities in relationship to the tDCS, the adverse events were comparable ($Z = -1.760$, $P = 0.078$; $Z = -0.439$, $P = 0.660$). The median for stimulation intensities and the electrode types was 1 (Fig. 6). Since there was no significant time effect ($P > 0.05$) on the VAS data (VAS collected every 2 min during each stimulation session), the time data sets were collapsed together and analyzed for

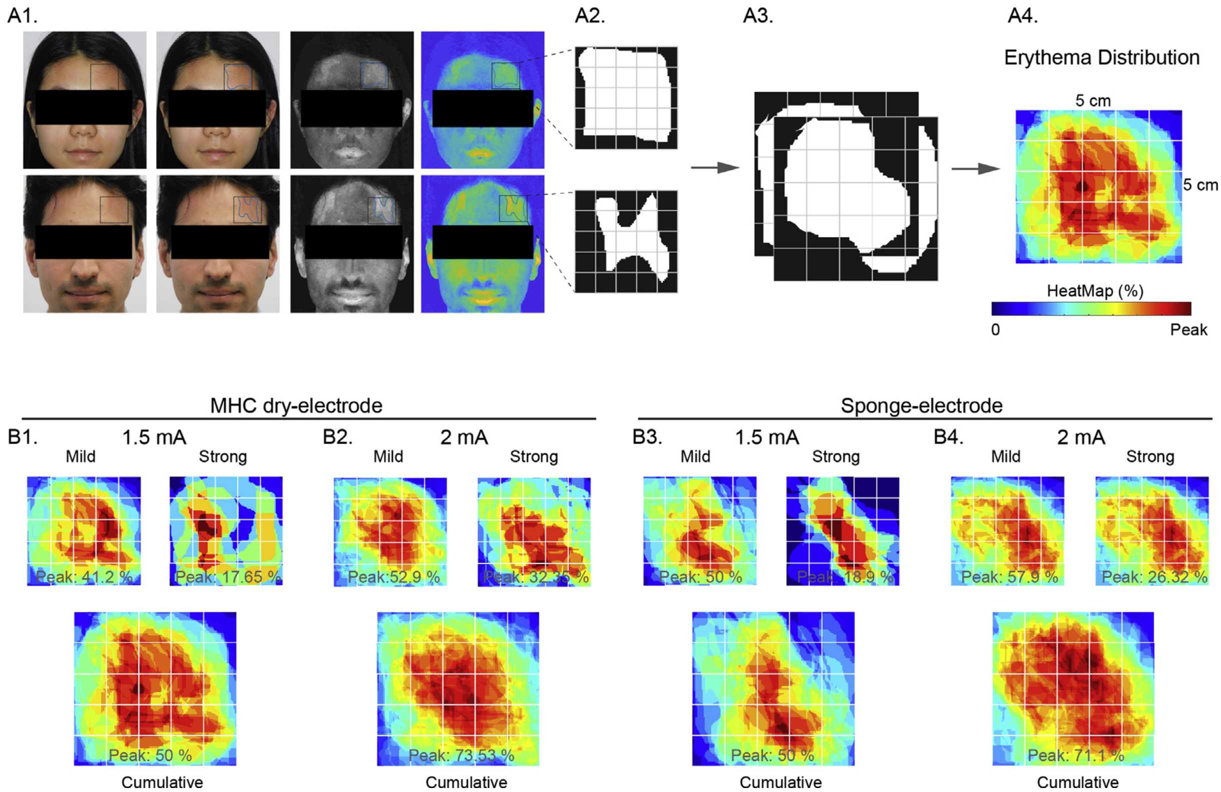

Fig. 4. Graphical representation of skin redness (erythema) distribution over the site of stimulation after tDCS (20 min, 1.5 mA, and 2 mA). (A1) depicts the image analysis steps where photographs of participants taken immediately after stimulation were passed through series of filters to isolate erythema region from the site of stimulation by defining a region of interest (ROI). (A2) represents a binary mask of erythema image traced by the rater. (A3) shows steps of computing the probability of erythema distribution by stacking all binary erythema mask. (A4) illustrates the mean heatmap of erythema distribution across subjects represented as a percentage across the ROI. Peak represent 100% probability in the color bar and probability was depicted as mild, strong, and combined heatmaps. (B1, B2) are erythema heatmaps of 1.5 mA and 2 mA using MHC dry electrode and (B3, B4) represents heatmaps for sponge-electrode. Combined erythema distribution was widely diffused with a comparable peak probability of erythema in both electrode types. (For interpretation of the references to color in this figure legend, the reader is referred to the Web version of this article.)

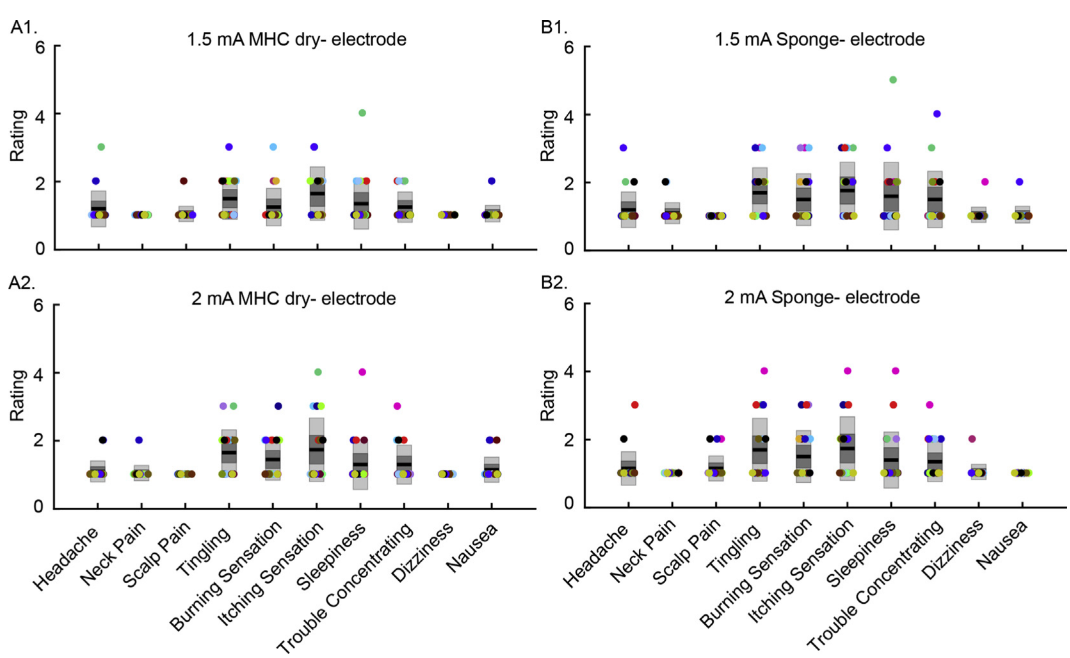

Fig. 5. Representation of adverse events for both MHC dry-electrode and sponge-electrode across stimulation intensities (1.5 mA and 2 mA) on a scale of 1–5; 1: none, 5: max. Participants are color-coded. The highest incidence of adverse events across all treatment groups were skin tingling, burning, and itching sensations (A1, A2, B1, B2). There was no statistically significant difference ($P > 0.05$) in adverse events between stimulation intensities, however between the electrode types, there was a significant difference ($P < 0.05$): less adverse events reported in the MHC dry-electrode. (For interpretation of the references to color in this figure legend, the reader is referred to the Web version of this article.)

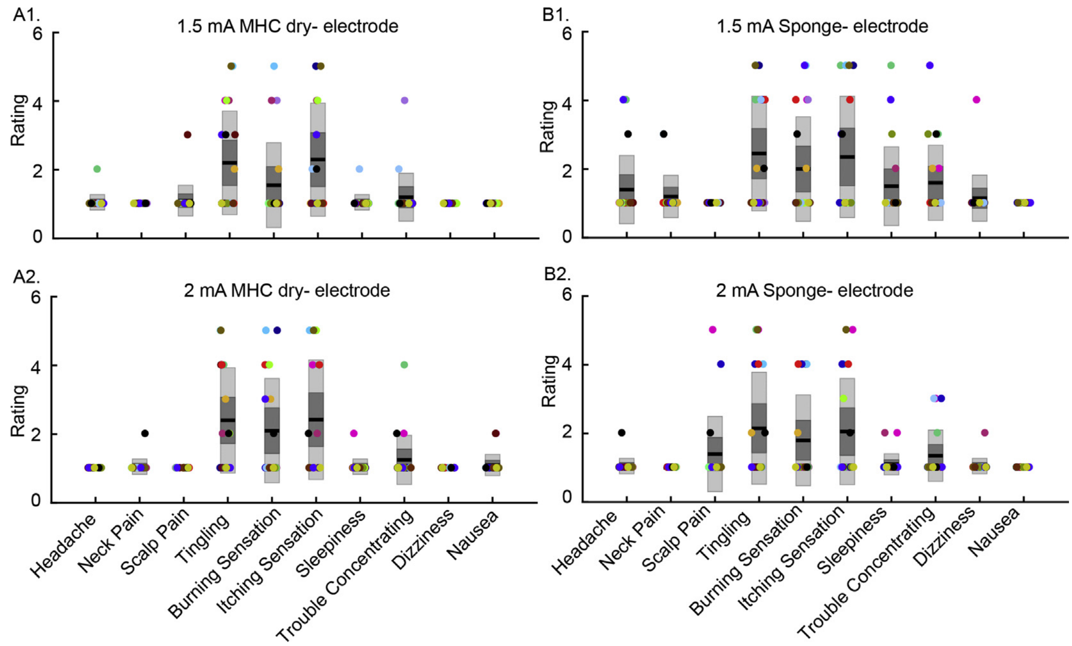

Fig. 6. Adverse events reporting for MHC dry-electrode and sponge-electrode at different stimulation intensities for relationship to tDCS. There was no significant difference ($P > 0.05$) in adverse events between conventional sponge-electrode (B1, B2) and MHC dry-electrode (A1, A2), and the stimulation intensities (1.5 mA V 2 mA).

statistical significance. The VAS pain score was higher in the sponge-electrode ($Mdn = 2$) than the MHC dry-electrode ($Mdn = 1.5$) ($Z = 5.341$, $P = 1.41e^{-7}$), whereas across the stimulation intensities (1.5 mA ($Mdn = 2$), 2 mA ($Mdn = 2$)), the VAS pain score was comparable ($Z = -0.567$, $P = 0.571$) (Fig. 7).

4. Discussion

We first defined a dry-electrode as 1) excluding any liquid of viscous electrolyte (as typical for conventional tDCS and HD-tDCS electrodes [8]) with the benefit of no accidental spread and no residue; 2) excluding any adhesive at the skin interface (common in

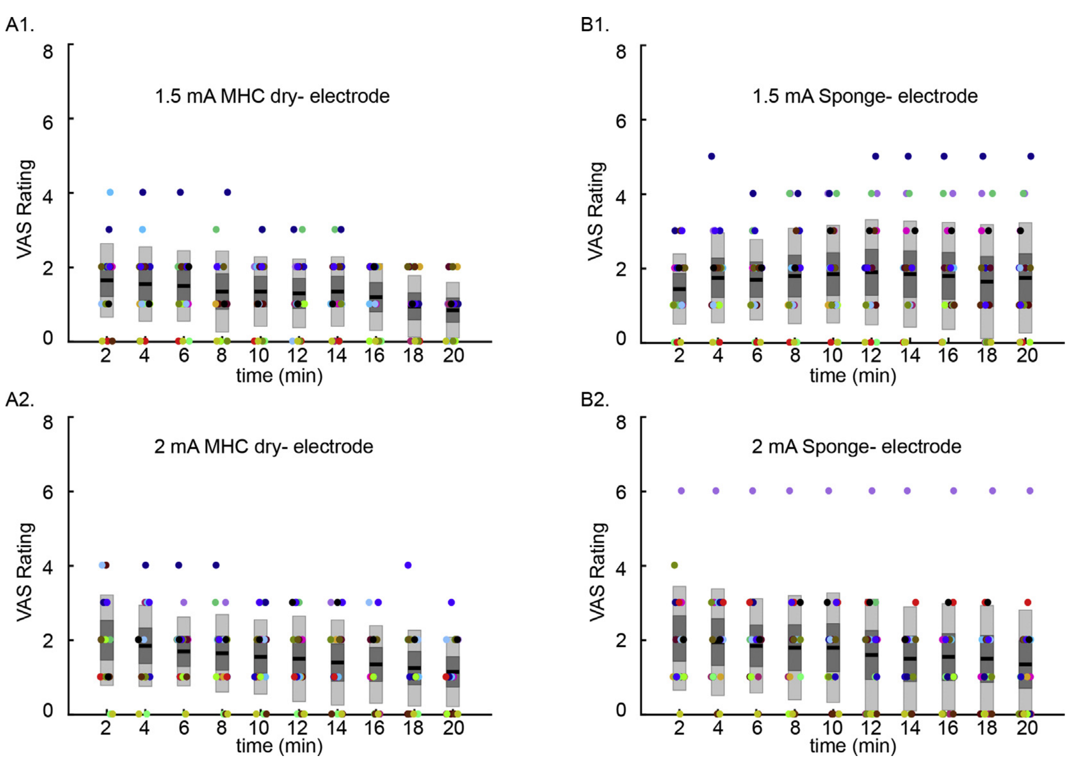

Fig. 7. VAS rating at different stimulation intensities (1.5 mA and 2 mA) for a conventional sponge and MHC dry electrode. Participants (20) were color-coded as the cumulative adverse events and relationship to tDCS data, and the VAS pain score (1–10 scale; 1: no pain, 10: unbearable pain) was collected every 2 min during each stimulation sessions. There was no significant different ($P < 0.05$) in the VAS rating across all four stimulation sessions. (For interpretation of the references to color in this figure legend, the reader is referred to the Web version of this article.)

TENS but rare for tDCS [4]) either integrated into or around the electrolyte; and 3) excluding any electrode preparation steps, even just saturation, except connection to the stimulator (which is an implicit step for a swapping disposable electrodes). A Multilayer Hydrogel Composite (MHC) dry-electrode design which satisfied these basic criteria was developed and then the electrode performance was verified in terms of current delivery and tolerability. For the conditions tested here, the MHC-electrodes performed sufficiently based on the improved VAS and comparable adverse event reporting, when compared to the conventional sponge-electrodes.

Focused on tDCS technology, we did not test any additional stimulation waveforms in this study. But tDCS is considered demanding from an electrode design standpoint [25] - for example, charge balanced pulses waveforms can be applied with conventional adhesive hydrogel electrodes while tDCS requires specialized electrodes [4] - so our success with tDCS is encouraging for additional waveforms. Still, only empirical testing can ultimately validate tolerability for each waveform and electrode design. In addition, we evaluated performance only below the hair line (SO positions) whereas tDCS is typically applied with at least one electrode above the headline (e.g. the common M1-SO montage). At a minimum, the MHC dry-electrodes may already be used below the hair line (e.g. SO) and a wet electrode above (e.g. M1). Noting the diffusivity of tDCS, other common montages, such as bifrontal positions [33] [34], may be emulated by lowering the electrode below the hairline, without necessarily compromising brain current flow [35]. Notwithstanding these questions, our results may encourage future work on the design and applications of dry-electrode stimulation.

Conflicts of interest

The City University of New York (CUNY) has IP on neurostimulation system and methods with author, Niranjan Khadka and Marom Bikson as inventors. Marom Bikson has equity in Soterix Medical Inc. Kiwon Lee is a co-founder of Ybrain Inc.

Acknowledgement

Source(s) of financial support: This study was partially funded by grants to MB from NIH (NIH-NINDS 1R01NS101362, NIH-NIMH 1R01MH111896, NIH-NCI U54CA137788/U54CA132378, and NIH-NIMH 1R01MH109289).

References

[1] Nitsche MA, et al. Transcranial direct current stimulation: state of the art 2008. Brain Stimul Jul. 2008;1(3):206–23.
[2] Bikson M, et al. Rigor and reproducibility in research with transcranial electrical stimulation: an NIMH-sponsored workshop. Brain Stimul Jun. 2018;11(3):465–80.
[3] Antal A, et al. Low intensity transcranial electric stimulation: safety, ethical, legal regulatory and application guidelines. Clin Neurophysiol 2017;128(9): 1774–809.
[4] Paneri B, et al. Tolerability of repeated application of transcranial electrical stimulation with limited outputs to healthy subjects. Brain Stimul Oct. 2016;9(5):740–54.
[5] Aparício LVM, Guarienti F, Razza LB, Carvalho AF, Fregni F, Brunoni AR. A systematic review on the acceptability and tolerability of transcranial direct current stimulation treatment in neuropsychiatry trials. Brain Stimul Oct. 2016;9(5):671–81.
[6] Bikson M, et al. Safety of transcranial direct current stimulation: evidence based update 2016. Brain Stimul Oct. 2016;9(5):641–61.
[7] Fertonani A, Ferrari C, Miniussi C. What do you feel if I apply transcranial electric stimulation? Safety, sensations and secondary induced effects. Clin Neurophysiol Nov. 2015;126(11):2181–8.
[8] Woods AJ, et al. A technical guide to tDCS, and related non-invasive brain stimulation tools. Clin Neurophysiol Feb. 2016;127(2):1031–48.
[9] Wang J, Wei Y, Wen J, Li X. "Skin burn after single session of transcranial direct current stimulation (tDCS). Brain Stimul Feb. 2015;8(1):165–6.
[10] Shiozawa P, et al. "Safety of repeated transcranial direct current stimulation in impaired skin: a case report. J ECT Jun. 2013;29(2):147–8.
[11] Poreisz C, Boros K, Antal A, Paulus W. Safety aspects of transcranial direct current stimulation concerning healthy subjects and patients. Brain Res Bull May 2007;72(4–6):208–14.
[12] Bikson M, Datta A, Elwassif M. Establishing safety limits for transcranial direct current stimulation. Clin Neurophysiol Jun. 2009;120(6):1033–4.
[13] Brunoni AR, Amadera J, Berbel B, Volz MS, Rizzerio BG, Fregni F. A systematic review on reporting and assessment of adverse effects associated with transcranial direct current stimulation. Int J Neuropsychopharmacol Sep. 2011;14(8):1133–45.
[14] Minhas P, Datta A, Bikson M. Cutaneous perception during tDCS: role of electrode shape and sponge salinity. Clin Neurophysiol Apr. 2011;122(4): 637–8.
[15] Brunoni AR, et al. Clinical research with transcranial direct current stimulation (tDCS): challenges and future directions. Brain Stimul Jul. 2012;5(3):175–95.
[16] Woods AJ, Bryant V, Sacchetti D, Gervits F, Hamilton R. Effects of electrode drift in transcranial direct current stimulation. Brain Stimul Jun. 2015;8(3): 515–9.
[17] Charvet L, et al. Remotely supervised transcranial direct current stimulation increases the benefit of at-home cognitive training in multiple sclerosis. Neuromodulation: Technol.Neural Interface Feb. 2017;21(4):383–9.
[18] Kronberg G, Bikson M. Electrode assembly design for transcranial Direct Current Stimulation: a FEM modeling study. Conf Proc IEEE Eng Med Biol Soc 2012:891–5. 2012.
[19] DaSilva AF, Volz MS, Bikson M, Fregni F. Electrode positioning and montage in transcranial direct current stimulation. JoVE May 2011;(51).
[20] Ambrus GG, Antal A, Paulus W. Comparing cutaneous perception induced by electrical stimulation using rectangular and round shaped electrodes. Clin Neurophysiol Apr. 2011;122(4):803–7.
[21] Knotkova H, et al. Automatic m1-so montage headgear for transcranial direct current stimulation (TDCS) suitable for home and high-throughput in-clinic applications. Neuromodulation May 2018. https://doi.org/10.1111/ner.12786 [Epub ahead of print].
[22] Orlov ND, et al. Stimulating thought: a functional MRI study of transcranial direct current stimulation in schizophrenia. Brain Sep. 2017;140(9):2490–7.
[23] Datta A, Bansal V, Diaz J, Patel J, Reato D, Bikson M. Gyri-precise head model of transcranial direct current stimulation: improved spatial focality using a ring electrode versus conventional rectangular pad. Brain Stimul Oct. 2009;2(4): 201–7. 207.e1.
[24] Minhas P, et al. Electrodes for high-definition transcutaneous DC stimulation for applications in drug-delivery and electrotherapy, including tDCS. J Neurosci Meth Jul. 2010;190(2):188–97.
[25] Merrill DR, Bikson M, Jefferys JGR. Electrical stimulation of excitable tissue: design of efficacious and safe protocols. J Neurosci Meth Feb. 2005;141(2): 171–98.
[26] Ezquerro F, et al. The influence of skin redness on blinding in transcranial direct current stimulation studies: a crossover trial. Neuromodulation: Technol.Neural Interface Apr. 2017;20(3):248–55.
[27] Smith D. Agarose gel electrophoresis. In: Murphy D, Carter D, editors. Transgenesis techniques. Humana Press; 1993. p. 433–8.
[28] Khadka N, Zannou AL, Zunara F, Truong DQ, Dmochowski J, Bikson M. Minimal heating at the skin surface during transcranial direct current stimulation. Neuromodulation: Technol.Neural Interface Jan. 2017;21(4):334–9.
[29] Caccavo D, Cascone S, Lamberti G, Barba AA. Hydrogels: experimental characterization and mathematical modelling of their mechanical and diffusive behaviour. Chem Soc Rev Apr. 2018;47(7):2357–73.
[30] Khadka N, Truong DQ, Bikson M. Principles of within electrode current steering. J. Med. Devices Jun. 2015;9(2). 020947–020947–2.
[31] Opitz A, Paulus W, Will S, Antunes A, Thielscher A. Determinants of the electric field during transcranial direct current stimulation. Neuroimage Apr. 2015;109:140–50.
[32] Miranda PC, Faria P, Hallett M. What does the ratio of injected current to electrode area tell us about current density in the brain during tDCS? Clin Neurophysiol Jun. 2009;120(6):1183–7.
[33] Brunoni AR, et al. Trial of electrical direct-current therapy versus escitalopram for depression. N Engl J Med 2017;376(26):2523–33. 29.
[34] Sampaio-Junior B, et al. Efficacy and safety of transcranial direct current stimulation as an add-on treatment for bipolar depression: a randomized clinical trial. JAMA Psychiatry Feb. 2018;75(2):158–66.
[35] Seibt O, Brunoni AR, Huang Y, Bikson M. The pursuit of DLPFC: non-neuronavigated methods to target the left dorsolateral pre-frontal cortex with symmetric bicephalic transcranial direct current stimulation (tDCS). Brain Stimul Jun. 2015;8(3):590–602.